

Free decay of shape oscillations of bubbles acoustically trapped in water and sea water

By THOMAS J. ASAKI AND PHILIP L. MARSTON

Department of Physics, Washington State University, Pullman, Washington, 99164-2814, USA

(Received 28 March 1995 and in revised form 24 May 1995)

Asymptotic results for the free decay of shape oscillations of viscous liquid spheres have been extended to include higher-order terms in the ratios of the inner and outer viscous penetration lengths to the radius. The new expressions are shown to be important for studies in which the two fluids have dissimilar densities and viscosities such as air/liquid systems. The analysis also includes an expansion for the frequency of maximum response of driven oscillations. The calculations are supported by measurements of the small-amplitude quadrupole mode free decay of nearly spherical bubbles acoustically levitated in clean water. The bubble radii ranged from 400 μm to 1400 μm . The results are interpreted in light of the initial-value problem. The lack of excess damping suggests that the interface behaves ideally for times up to two hours after bubble injection. Measurements were also carried out on bubbles in 0.5 M NaCl solution and in sea water. Larger bubbles (radius $> 800 \mu\text{m}$) in clean water exhibit damping two to four times larger than predicted by theory. The transition from this anomalous damping to theoretical damping is a very abrupt function of radius. All observations were carried out with similar acoustic fields for counteracting buoyancy. The excess damping appears to be associated with some nonlinear response of the bubble.

1. Introduction

The study of the dynamics of fluid drops and air bubbles suspended in a host medium is important for a wide variety of applications. The behaviour of air bubbles and liquid drops is important for materials processing applications (purification of liquids, bubbly flows, chemical reactions, etc.) especially in low-gravity environments. The behaviour of sea bubbles is known to have important effects on climate and health (Horne 1969; Monahan & Van Patten 1989). Small bubbles are important in the study of cavitation phenomena and sonoluminescence (Young 1989; Crum 1994). Nonlinear coupling of shape and volume modes has been of considerable interest (Longuet-Higgins 1992; Yang, Feng & Leal 1993). Acoustic levitation has been found to be an effective method for trapping and positioning the samples for study. It is also possible to induce shape oscillations of samples through amplitude modulation of the acoustic radiation pressure (Marston & Apfel 1979; Trinh, Zwern & Wang 1982). In this way, forced or freely decaying oscillations can be conveniently studied in a variety of situations. For example, this method has been used to measure interfacial properties (Marston & Apfel 1980; Hsu & Apfel 1985; Trinh, Marston & Robey 1988; Lu & Apfel 1990). The levitation and shape oscillation of millimetre size bubbles has also been demonstrated (Asaki, Marston & Trinh 1993).

The emphasis of this paper is on the free decay of shape oscillations of bubbles. An extension of previous theoretical models (Miller & Scriven 1968; Marston 1980;

Prosperetti 1980*a*) is derived which more accurately describes the dynamics of gas bubbles in a liquid and the dynamics of liquid drops in air. In addition to solutions of the characteristic equation, experimental work is presented in support of the new calculations; namely, measurements of the free decay of small-amplitude quadrupole shape oscillations of bubbles in clean water. A difficulty with these experiments is that trapping of the sample against its buoyancy induces a static oblate shape. For sufficiently small bubbles trapped in water, however, the equilibrium shapes can have aspect ratios very near unity (Asaki & Marston 1995). The effects of the weak static background distortion of the bubble (typically 1% of the radius) are approximated by linear superposition of the distortion on the small-amplitude oscillations about a spherical shape (Marston 1980).

The characteristic equation for the decay of shape oscillations is found by linearization of the Navier–Stokes equation and requires that the amplitude of distortions is small compared to the bubble or drop size (Miller & Scriven 1968; Marston 1980; Prosperetti 1980*b*). The fluids are assumed to have Newtonian behaviour and the interfacial region is considered to be ideal (no interfacial viscosity or elasticity). Dissipation of energy arises from normal viscous dissipation away from the interface as well as in an oscillating viscous boundary layer. The form of the characteristic equation is sufficiently complicated that it may be solved with asymptotic expansions or numerically. Asymptotic approximations given previously reveal viscous corrections to Lamb's (1932) inviscid expression (Miller & Scriven 1968; Marston 1980; Prosperetti 1980*a*; Hsu & Apfel 1987; Lu & Apfel 1990). The expansions, extended in the present analysis, illustrate the significance of the damping mechanisms. The resulting linear damping rates may give insight into the importance of nonlinear mode coupling rates approximated for bubbles in inviscid fluids (Longuet-Higgins 1992; Yang *et al.* 1993).

This paper is organized as follows. The theoretical analysis extends the previous asymptotic solution for the free decay of shape oscillations. Comparison with numerical solutions in representative cases shows that new terms in the analytical approximation are especially significant in the case of shape oscillations of gas bubbles in liquids and, to a lesser extent, drops of liquid in a gas. The experimental set-up and procedures are described, including the preparation of materials and the data reduction procedures. Experimental results are presented for the free decay of quadrupole oscillations of air bubbles in pure water and in 0.5 M NaCl solution. The results are discussed in light of the extended calculations. Results are shown for a bubble in sea water which exhibits excess damping. Various expansions and parameters used in the approximate results are outlined in Appendix A. The maximum response frequency for the case of acoustically forced oscillations is expanded in Appendix B. That analysis is germane to the initial conditions used in the measurement of the free decay.

2. Theory

This section examines the extended approximation for the free decay of shape oscillations of drops or bubbles about a spherical shape. The extended approximation is found to more accurately describe situations in which the host medium and sample have very different densities and viscosities. The new expressions are compared in turn with numerical solutions and the applicability of each is discussed. This section finishes with a discussion of the initial-value problem and the implications for conducting free-decay measurements.

2.1. Complex free-decay frequency

It is appropriate to review the evolution of the shape for the linearized description of freely decaying normal modes of a spherical drop or bubble. For the purpose of this discussion it is sufficient to restrict attention to axisymmetric modes such that the instantaneous surface is given by

$$\tilde{R}(\theta, t) = \tilde{R}_0 \left\{ 1 + \sum_{n=2}^{\infty} \operatorname{Re} [x_n \exp(i\Omega_n t)] P_n(\cos \theta) \right\}, \quad (1)$$

where P_n is a Legendre polynomial of the indicated argument, θ is the polar angle, x_n is the complex modal amplitude, and \tilde{R}_0 is the equilibrium radius of the bubble or drop. The complex frequency Ω_n describes the period and decay rate of the n th mode. It is convenient to suppress the mode index n except when needed for clarity. Under the restriction of incompressible potential flow, the characteristic equation is found by applying standard boundary conditions to the linearized Navier–Stokes equation. The result can be represented as a determinant (Marston 1980):

$$\begin{vmatrix} -i\Omega & 1 & 0 & 0 & 0 \\ 0 & 1 & 0 & -1 & 0 \\ 0 & -(n-1) & z_i \mathcal{Q}_n^j & -(n+2) & 2n+1 - z_o \mathcal{Q}_n^h \\ \frac{-\omega^2 \Gamma R^2}{n(n+1)} & \frac{\mu_i z_i^2}{n} - 2(n-1)\mu_i & -\frac{\mu_i z_i^2}{n} + 2\mu_i z_i \mathcal{Q}_n^j & \frac{\mu_o z_o^2}{n+1} - 2(n+2)\mu_o & -\frac{\mu_o z_o^2}{n+1} + 2(2n+1)\mu_o - 2\mu_o z_o \mathcal{Q}_n^h \\ 0 & 2(n^2-1)\mu_i & -\mu_i z_i^2 + 2\mu_i z_i \mathcal{Q}_n^j & -2n(n+2)\mu_o & -\mu_o z_o^2 + 2(2n+1)\mu_o - 2\mu_o z_o \mathcal{Q}_n^h \end{vmatrix} = 0. \quad (2)$$

This expression is equivalent to those of Miller & Scriven (1968) and Prosperetti (1980*a*). Here ω is the frequency for the inviscid case (Lamb 1932):

$$\omega = \frac{1}{2\pi} \left(\frac{\sigma n(n+1)(n-1)(n+2)}{R^3 \Gamma} \right)^{1/2}, \quad (3)$$

where $\Gamma = n\rho_o + (n+1)\rho_i$, σ is the interfacial tension, μ_o and μ_i are the outer and inner fluid viscosities respectively, and ρ_o and ρ_i are the outer and inner fluid densities respectively. The symbols \mathcal{Q}_n^j and \mathcal{Q}_n^h are defined as ratios of spherical Bessel functions and spherical Hankel functions of the first kind respectively:

$$\mathcal{Q}_n^j \equiv \frac{j_{n+1}(z_i)}{j_n(z_i)}, \quad \mathcal{Q}_n^h \equiv \frac{h_{n+1}^{(1)}(z_o)}{h_n^{(1)}(z_o)}, \quad (4)$$

where
$$z_o = (i-1) R \left(\frac{\Omega \rho_o}{2\mu_o} \right)^{1/2}, \quad z_i = (i-1) R \left(\frac{\Omega \rho_i}{2\mu_i} \right)^{1/2} \quad (5)$$

Equation (2) can be simplified by considering the leading-order viscous corrections in the limit $|z_o|, |z_i| \gg 1$. The resulting characteristic equation is

$$\omega^2 - \Omega^2 + i(1+i)\alpha\Omega^{3/2} + i\gamma\Omega - (1+i)\kappa\Omega^{1/2} + i(1+i)\delta + \dots = 0. \quad (6)$$

The particulars of the asymptotic expansions and the fluid-property dependent parameters α , γ and κ are discussed in Appendix A. The parameter δ has not been explicitly determined except to note the complex nature of the term in equation (6).

| Sample radius | 0.3 mm | 1.0 mm | 3.0 mm |
|--------------------------------------|---------------|----------------|----------------|
| Water drop in air | | | |
| Equation (9) | 4620 + 52.70i | 759.3 + 4.838i | 146.1 + 0.550i |
| Equation (8) | 4618 + 50.85i | 759.2 + 4.715i | 146.1 + 0.540i |
| Equation (2) | 4618 + 50.81i | 759.1 + 4.713i | 146.1 + 0.540i |
| <i>p</i>-Xylene drop in water | | | |
| Equation (9) | 2562 + 155.7i | 427.1 + 18.42i | 82.99 + 2.639i |
| Equation (8) | 2562 + 155.8i | 427.1 + 18.43i | 82.99 + 2.639i |
| Equation (2) | 2563 + 157.2i | 427.2 + 18.52i | 83.00 + 2.647i |
| Air bubble in water | | | |
| Equation (9) | 5651 + 200.7i | 929.2 + 18.22i | 178.9 + 2.046i |
| Equation (8) | 5637 + 183.3i | 928.2 + 17.06i | 178.8 + 1.948i |
| Equation (2) | 5638 + 183.5i | 928.2 + 17.07i | 178.8 + 1.949i |
| Equation (B 1) | 5635 | 928.0 | 178.8 |
| Equation (B 3) | 5630 | 927.8 | 178.8 |

TABLE 1. Calculated complex free decay Ω (rad s⁻¹) for quadrupole shape oscillations of a spherical sample. Representative cases are considered for three different systems: a water drop in air; a *p*-xylene drop in water; and an air bubble in water. For each case three different sample radii are considered and the response is calculated by three methods described in the text. In addition, the frequency of maximum response for driven oscillations is shown for an air bubble in water as calculated numerically (B 1), and approximated by (B 3).

This form of the characteristic equation was given by Marston (1980) up to and including the γ dependent term. It is noteworthy that equation (6) (and thus all of the results that follow) can be obtained from Marston's expression by the substitution $\alpha \rightarrow \alpha + i\kappa/\Omega + \delta/\Omega^{3/2}$. Equation (6) was solved using Newton's method of iteration with the initial value $\Omega = \omega$. The result is

$$\Omega = \omega - \frac{\alpha\omega^{1/2}}{2} + \frac{7\sqrt{2}\alpha^3}{32\omega^{1/2}} - \frac{3\alpha\gamma}{8\omega^{1/2}} - \frac{\kappa}{2\omega^{1/2}} - \frac{5\alpha^4}{32\omega} + \frac{3\alpha\gamma}{8\omega} - \frac{\gamma^2}{8\omega} - \frac{\alpha\kappa}{2\omega} - \frac{\delta}{2\omega} + i\left(\frac{\alpha\omega^{1/2}}{2} - \frac{\alpha^2}{2} + \frac{\gamma}{2} + \frac{7\sqrt{2}\alpha^3}{32\omega^{1/2}} - \frac{3\alpha\gamma}{8\omega^{1/2}} - \frac{\kappa}{2\omega^{1/2}} + \frac{\delta}{2\omega}\right) + O(\omega^{-3/2}). \quad (7)$$

The real part of Ω is the free-decay frequency. The imaginary part of Ω is the decay constant (reciprocal of the decay time constant). Terms involving $\alpha\omega^{1/2}$ have the form of viscous shear layer dissipation near the interface. The parameter γ is descriptive of damping directly proportional to the generalized velocity of the n th mode. The relative importance of each term will depend upon the system under investigation. While some of the terms will always be small, they have been included here for completeness. We find that, for a wide variety of systems, Ω is approximated well by

$$\Omega \approx \omega - \frac{\alpha\omega^{1/2}}{2} - \frac{3\alpha\gamma}{8\omega^{1/2}} - \frac{\kappa}{2\omega^{1/2}} - \frac{\gamma^2}{8\omega} + i\left(\frac{\alpha\omega^{1/2}}{2} - \frac{\alpha^2}{2} + \frac{\gamma}{2} - \frac{3\alpha\gamma}{8\omega^{1/2}} - \frac{\kappa}{2\omega^{1/2}}\right). \quad (8)$$

This expression retains only the leading-order α , γ and κ corrections. With the further omission of the κ terms, Marston's (1980) expression is recovered:

$$\Omega \approx \omega - \frac{\alpha\omega^{1/2}}{2} - \frac{3\alpha\gamma}{8\omega^{1/2}} - \frac{\gamma^2}{8\omega} + i\left(\frac{\alpha\omega^{1/2}}{2} - \frac{\alpha^2}{2} + \frac{\gamma}{2} - \frac{3\alpha\gamma}{8\omega^{1/2}}\right), \quad (9)$$

where a transcription error in the $\alpha\gamma\omega^{-1/2}$ term of the previous work is corrected.

| Fluid | Property | Value |
|------------------|---------------------|--|
| Air | ρ | 0.001 075 g cm ⁻³ |
| | μ | 0.000 184 g s ⁻¹ cm ⁻¹ |
| Water | ρ | 0.9970 g cm ⁻³ |
| | μ | 0.008 905 g s ⁻¹ cm ⁻¹ |
| | σ | 71.97 dyn cm ⁻¹ |
| <i>p</i> -Xylene | (relative to air) | |
| | ρ | 0.857 g cm ⁻³ |
| | μ | 0.006 14 g s ⁻¹ cm ⁻¹ |
| | σ | 37.5 dyn cm ⁻¹ |
| | (relative to water) | |

TABLE 2. Physical properties of fluids at 25 °C where ρ is the density, μ is the viscosity, and σ is the interfacial tension. The elevation of the laboratory is 780 m and the local acceleration due to gravity is 981 cm s⁻².

The applicability of the various approximations in this section are examined with respect to three specific cases: a water drop in air; a drop of *p*-xylene in water; and an air bubble in water. These examples are representative of a wide variety of fluid–fluid systems. In each case the complex free decay has been calculated by three methods: the former result of Marston, equation (9); the newly proposed approximate solution, equation (8); and the numerical solution of equation (2). The results are shown in table 1 and the physical parameters used in the calculations are given in table 2. The important results are:

(i) In all cases the complex frequency obtained through equation (8) closely approximates the numerical result. Larger deviations are associated with smaller sample sizes.

(ii) For dissimilar fluids, such as water drops in air and air bubbles in water, the leading order κ term in (8) represents a significant adjustment to the damping constant as given by (9). Deviations of several per cent are evident for small bubbles in water. Somewhat smaller corrections are present for the case of water drops in air.

(iii) For dissimilar fluids the leading-order κ term represents a minor adjustment to the free-decay frequency. The largest differences are associated with small air bubbles in water.

(iv) For fluids of similar densities and viscosities, such as *p*-xylene and water, the leading order κ terms are not significant. The numerical results for the frequency and damping constant are accurately predicted by both equations (8) and (9). Small discrepancies are present in the decay constant and appear to grow with decreasing sample size.

2.2. The initial-value problem

The response of an initially deformed sample in a fluid is an initial-value problem (Prosperetti 1980*a, b*); the decay towards spherical equilibrium depends upon the initial bulk fluid flow field as well as the sample's initial shape. The free decay is not necessarily fully described by equation (1) with a time independent Ω_n as has been assumed in the previous analyses. For example, a sample which is deformed in a static fluid will undergo an initially aperiodic decay which approaches periodicity only as the flow field becomes sufficiently developed. However, a sample which is initially driven at the free-decay frequency will exhibit periodic decay when the driving mechanism is removed. In this case, the flow fields are in a dynamic initial state which closely resembles the fully developed free-decay flow fields. From an experimental standpoint, this initial condition may at first appear impractical. The simplest procedure is to drive

oscillations at the easily observable frequency of maximum response ω^{max} (expressions are presented in Appendix B). Confidence in this approach is based upon how well ω^{max} approximates $\text{Re}(\Omega)$. For the case of bubbles in clean water this approximation is extremely good (see table 1). Thus, it is expected that a purely periodic decay will be evident for bubbles initially driven at the frequency of maximum response.

3. Experimental description

This section begins with a description of the acoustic levitation system and the basic operating considerations. The acoustic field is considered with respect to the tuning of the levitator and coupling into the bubble shape modes. The data collection methods are then described including bubble size and shape determination through a CCD camera image and bubble response detection techniques. Included in this section are materials preparation and data reduction procedures.

3.1. Levitation system

The acoustic levitation apparatus (figure 1) is very similar to those used in previous studies of levitated liquid and air samples (Asaki *et al.* 1993; Trinh *et al.* 1982). The construction materials were chosen, as far as possible, to minimize host liquid and sample contamination. The support structure is rectangular with a height of 15.9 cm and a square cross-section of side 10.2 cm. The upper portion is a water chamber constructed from 0.64 cm thick Plexiglas walls. The chamber is open at the top for easy access and water level adjustment. Typical water column height is 7.0 cm (volume is approximately 600 ml). The base is a Plexiglas block 8.25 cm tall from which a cylindrical bore 7.94 cm in diameter has been removed. The various pieces are bonded with a Plexiglas solvent. The base houses a hollow cylindrical piezoelectric transducer (0.64 cm thick, 7.62 cm o.d., 7.62 cm tall) held in place by a Viton O-ring at its midplane. The upper end of the transducer is capped by a 0.32 cm thick circular glass plate which provides the acoustic source. An aluminium ring is bonded to the glass plate in order to modify the resulting acoustic field providing improved lateral stability for levitated bubbles (Asaki *et al.* 1993). The host liquid contained by this apparatus comes into contact with the Plexiglas walls and base, the glass plate, the aluminium ring with epoxy, the upper half of the coated piezoelectric transducer, the O-ring, and the open air. The fully assembled levitator was cleaned with household dish soap and rinsed repeatedly with purified water. Plexiglas is thought to be only a weak source of contamination of the surface quality of water (Scott 1978).

3.2. Acoustics

The ultrasonic field used for levitation and bubble shape mode excitation is produced by driving the piezoelectric transducer near its fluid-loaded resonance of 22.8 kHz. Applied voltages are typically 4 V r.m.s. The transducer, while excited in a radial mode, provides vertical motion to the glass plate through Poisson coupling. The sound field near the axis of the levitator approximates a one-dimensional plane standing wave of one wavelength in the vertical direction (Asaki & Marston 1995). All of the water chamber boundaries closely approximate pressure release surfaces. The nature of the field away from the axis, though complicated, does not appear to introduce spurious acoustic radiation force effects (Asaki & Marston 1994). The axial pressure is a sinusoidal function consisting of a centrally located pressure nodal region and two regions of high pressure. The typical acoustic pressure amplitudes are 0.5 to 1.5 atm.

The levitator resonance (22.8 kHz) corresponds to the monopole resonance

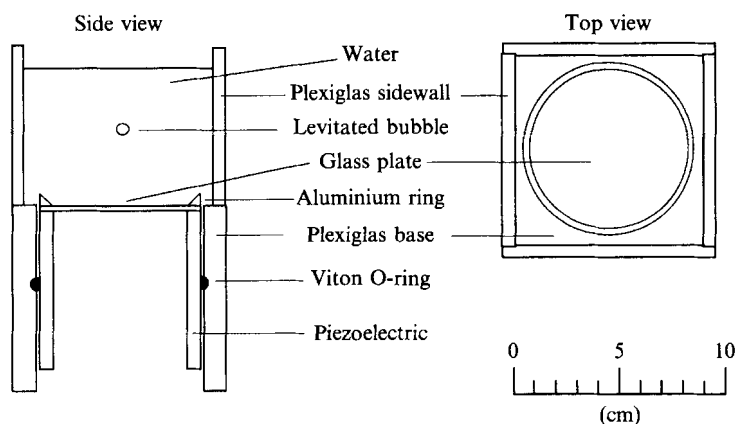


FIGURE 1. Schematic of the levitation apparatus showing the approximate location of a levitated air bubble. Construction details and acoustic features are discussed by Asaki *et al.* (1993) and Asaki & Marston (1994).

frequency of an air bubble of radius 140 μm . Bubbles of larger radius will be levitated near to and above pressure nodal regions while bubbles of smaller radius will be levitated near to and above pressure antinodal regions (Asaki *et al.* 1993). The bubbles observed in this study were trapped above the axial pressure node roughly in the centre of the water chamber. The radiation pressure which provides the levitation capability also distorts the bubble into an oblate shape. Nearly spherical bubbles are expected to have a primarily quadrupole distortion. Bubble stability in slightly degassed water was good both laterally and vertically. No difficulties were encountered either during the taking of pictures or during observation of shape mode decay. Some lateral bubble motion is discernible in real time CCD image observation. These motions are of the order of 1 Hz and should not affect data collection or analysis.

Shape mode oscillations are induced by the method of amplitude modulation of the radiation pressure. The voltage applied to the transducer, V , can be represented as

$$V = V_0[1 + \epsilon \cos(2\pi f_M t)][\cos(2\pi f_L t)], \quad (10)$$

where V_0 is the signal amplitude, f_L is the frequency of levitation (≈ 22.8 kHz), f_M is the frequency of amplitude modulation, and ϵ is the degree of modulation (100 ϵ is the modulation percentage). Observations show that no modulation threshold is required for inducing shape oscillations in agreement with similar studies for drops (Marston & Apfel 1980).

3.3. Materials preparation

Water used as the host liquid was processed in several stages. Local tap water was first de-ionized (resistivity ≈ 2 M Ω cm) and then fed into a Gilmont vertical distillation apparatus. The product (60 + $^{\circ}\text{C}$) was collected at a rate of one litre per hour directly into clean Teflon bottles. Full bottles were sealed with a Teflon cap and allowed to cool to room temperature. Cooling without atmospheric contact guarantees that the end product is somewhat degassed; solubility of nitrogen and other atmospheric gases is lowered at high temperatures. This degree of degassing has been found to be sufficient for inhibiting cavitation noise at the pressure amplitudes involved in levitating millimetre size bubbles. Bottles were kept sealed until the time of an experiment.

Molecular biology grade sodium chloride was obtained and further purified by melting in ceramic crucibles in a high temperature oven at 960 $^{\circ}\text{C}$. The salt was kept

molten for over three hours and then allowed to cool over a few hours to room temperature. After the salt was removed 59 g was weighed and placed in an empty two litre Teflon bottle. Water was collected hot directly into the bottle from the distillation apparatus and sealed when full. The water was then allowed to come to room temperature. In this way 0.5 M NaCl solution was produced which was somewhat degassed.

3.4. Bubble imaging and sizing

A CCD camera was employed for determining the size and shape of levitated bubbles. The images had a typical resolution of 20 μm /pixel dependent upon the extension of a bellows used for magnification. Exposure times of 15 ms were typical. The available CCD array measured 165 \times 192 pixels. High contrast bubble images were obtained by diffuse source backlighting.

The static size and shape of each bubble were found in the absence of modulation by the following method. The bubble image was passed through a modified-gradient edge-finding routine which locates a discrete point profile of the bubble. These points were then fitted to a Legendre polynomial function:

$$r(\theta) = R_0 + \sum_{n=2}^m R_n P_n(\cos \theta), \quad (11)$$

where r is the local bubble radius, θ is the polar angle, P_n is the Legendre polynomial of order n , R_n is the coefficient of P_n , and m is the maximum order used in the fitting procedure. It was found that $m = 2$ provided excellent profile fits; the bubbles were shown to have a primarily quadrupole distortion. Calibration checks by imaging stainless steel ball bearings demonstrate accuracy of the horizontal and vertical radii determination to within 0.5%. Uncertainties in bubble aspect ratio determination vary accordingly.

3.5. Free-decay detection system

The free decay was recorded by measuring the extinction of light caused by a bubble placed in the path of an expanded laser beam (figure 2). The technique is known as the pseudo-extinction method (Trinh *et al.* 1988; Lu & Apfel 1990; Stroud & Marston 1993, 1994). The expanded laser beam was aligned to pass vertically along the axis of the levitator. A focusing lens collected the light through an aperture onto a photodetector. For a vertical beam of light the cross-section of a bubble undergoing small-amplitude axisymmetric quadrupole shape oscillations is a circle whose radius varies sinusoidally about its equilibrium as illustrated in figure 2. The light power reaching the photodetector is reduced as the bubble cross-section becomes larger. For bubbles much larger than the wavelength of light the effective scattering cross-section is approximately $2\pi R^2$ (twice the cross-sectional area of the bubble). The scattered power is roughly equally divided into: (i) a forward diffraction contribution; and (ii) externally reflected and internally reflected and refracted contributions. The aperture was present to transmit the full forward-scattering diffraction peak while at the same time blocking the larger angle reflected and refracted contributions from reaching the photodetector. This approach allowed for ease of alignment and was insensitive to lateral bubble motion. The aperture size h was such that $h \gg \lambda f/R$ where λ is the wavelength of light (638 nm) and f the lens focal length (11 cm). The photodetector output for driven or decaying oscillations consisted of a small sinusoidal variation superimposed on a relatively large d.c. signal (total power minus (ii) contribution). This signal was amplified and sent through a high-pass filter. The result was recorded on a digital oscilloscope. The signal levels were more than sufficient for extracting the

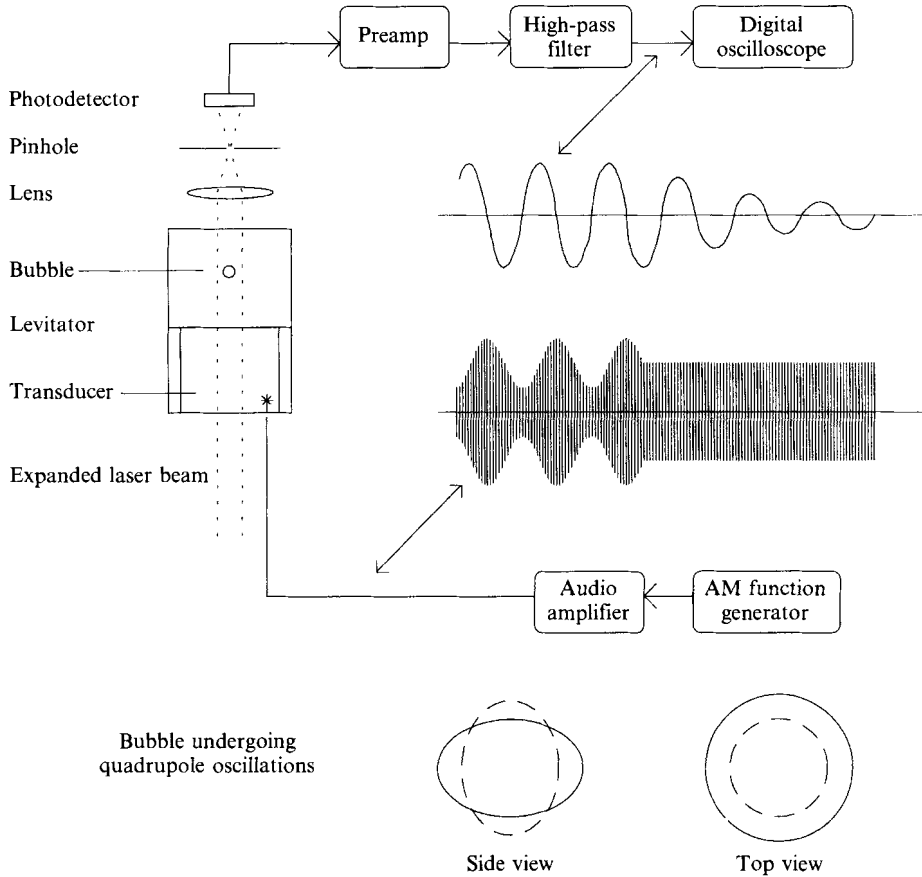


FIGURE 2. Experimental set-up. A levitated bubble is driven into small-amplitude shape oscillations by means of modulated acoustic radiation pressure. The free decay of the oscillations, subsequent to termination of the modulation, is recorded on a digital oscilloscope by means of the pseudo-extinction method (see text).

decay properties over the entire range of bubble sizes studied. It was necessary to use a low-noise laser according to the advice of Stroud & Marston (1993).

Data collected in this way was fitted to a pure exponential decay of a sinusoid with five free parameters:

$$v(t) = \Delta v + v_0 \cos(\omega t + \phi) \exp(-t/\tau), \quad (12)$$

where $v(t)$ is the filtered output voltage of the photodetector, Δv is an allowed small d.c. offset, v_0 is an amplitude, ω is the free-decay frequency, ϕ is an initial phase, and τ is the decay time (inverse of the damping constant). The fitting procedure initially includes all data points in the time window $-0.3\tau' < t < 3\tau'$ where τ' is an initial approximation based upon the raw data. The selected data is then fitted to equation (12) by a least-squares method in which the difference function minimum is reached by a linearized gradient approach. Next, a new data range is selected based upon the fit parameter τ , and the fitting procedure is repeated. The second fit yields the experimental values for the free-decay frequency ω and the free-decay damping constant $1/\tau$. Figure 3 shows a sample data trace and the final fit to a subset of the data.

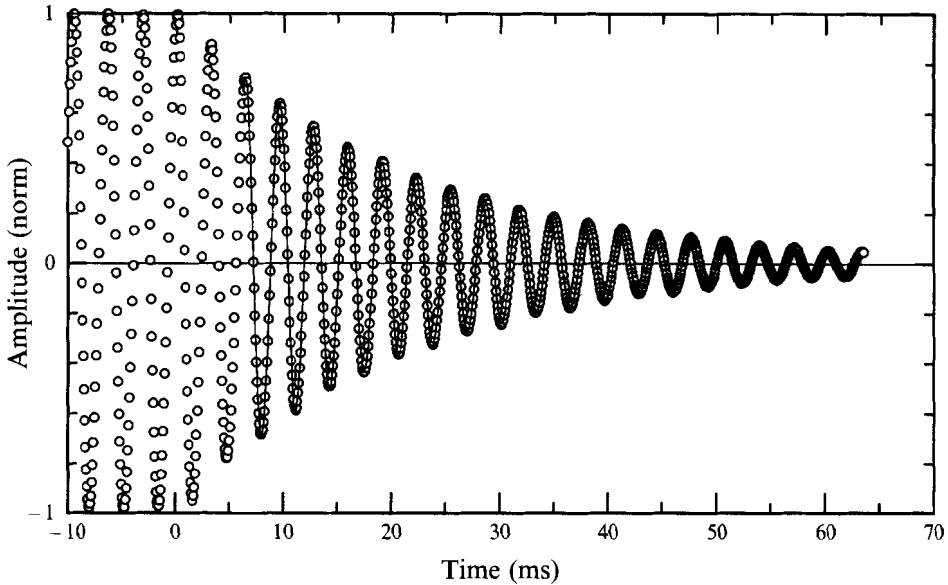


FIGURE 3. Sample data trace of the free decay of quadrupole oscillations for a bubble in clean water. The oscillations are driven by modulation of the acoustic radiation pressure up until the zero time. The open circles are the data and the solid line is an exponentially decaying sinusoid fitted to a subset of the data. The quality of the data and fit is in part due to the use of an intensity stabilized HeNe laser. In this example $\omega/2\pi = 292.3$ Hz, $\tau = 22.02$ ms, $R = 608.9$ μm , and $A = 1.006$.

4. Experimental procedure

An experiment involves the observation of a single levitated bubble over the course of several minutes or even up to a few hours. The procedure is as follows:

- (i) Prepare the host solution 12 to 24 hours prior to the beginning of the experiment. This allows temperature equilibration between fluid, room and levitator.
- (ii) Clean the glassware and thoroughly rinse the levitator with clean water just prior to beginning.
- (iii) Fill the levitator with the host fluid to a depth of 7.0 cm. Adjust levitator drive amplitude (without modulation) to 3.5 or 4.0 V r.m.s which is just sufficient for levitating bubbles of $R_0 \approx 1.5$ mm.
- (iv) Inject a test bubble by means of a glass microlitre pipette. Tune the levitator by adjusting the frequency of levitation so that the bubble is trapped at its lowest position. With the bubble in place, check the alignment of the optics. The bubble should be near to the centre of the laser beam. Remove the test bubble.
- (v) Select the desired modulation percentage, 100ϵ , such that the amplitude of shape oscillations is always small relative to the bubble size. Measurements of the amplitude can be made by the method described by Stroud & Marston (1993).
- (vi) Inject a bubble with the modulation off. Set experiment timer $t_e = 0$.
- (vii) Turn the amplitude modulation on. Adjust the modulation frequency so that the photodiode signal is maximized. The bubble is now being driven at its frequency of maximum response.
- (viii) Switch off the modulation. The digital scope records the free decay of the oscillations.
- (ix) Backlight the bubble and record the now static image. This step immediately follows step (viii). Record the experiment elapsed time t_e and the host fluid temperature.

(x) Repeat steps (vii) through (ix).

The length of an experiment depends upon the water's dissolved gas content. Solutions which are relatively near saturation dissolve bubbles more slowly than solutions which are in a largely gas-depleted state. The experiment is terminated when the gradually dissolving bubble shifts abruptly to a different levitation position. The host liquid may also become sufficiently regassed that the experiment is effectively ended by cavitation noise.

5. Results

Four representative experiments, each involving a single levitated air bubble, will be discussed. The first two experiments were carried out in purified water. The third experiment was carried out in a 0.5 M purified NaCl solution. A fourth experiment was carried out in a sea-water sample. All experiments were conducted at room temperature and an atmospheric pressure near 700 mmHg. This value of the pressure (0.92 atm.) is reduced from standard pressure owing to the elevation of the laboratory. Oscillation amplitudes have been measured for a few representative bubbles and have been found to be less than 10% of bubble radius in all cases. These small amplitudes are induced with acoustic pressure modulations of 10–40% ($0.1 < \epsilon < 0.4$). The data are presented in figures 4–8. The time evolution of the bubble properties are shown from the time of bubble injection up to the time the experiment is terminated. The equilibrium bubble shape is given by the aspect ratio A defined as:

$$A = \frac{r(\theta = \frac{1}{2}\pi)}{r(\theta = 0)}, \quad (13)$$

from (11) with $m = 2$. The radiation pressure distribution on the bubble is such that its static shape is slightly oblate. For the purpose of theoretical analysis, the bubble size is given by the volume equivalent radius R which is the radius of a sphere of the same volume as the bubble:

$$R = \left[\frac{1}{2} \int_0^\pi r^3(\theta) \sin(\theta) d\theta \right]^{1/3}. \quad (14)$$

This characterization is equivalent to the approximation that the effects of static background distortion and of small-amplitude oscillations about a spherical shape can be added by linear superposition (Marston 1980). The free decay frequency of quadrupole shape oscillations is described by the dimensionless quantity F which is defined as the ratio of the experimental to theoretical frequencies:

$$F \equiv \frac{\omega}{\text{Re}(\Omega)}. \quad (15)$$

The free-decay damping constant is described by the dimensionless quantity S which is defined as the ratio of the experimental to theoretical damping constants:

$$S \equiv \frac{1/\tau}{\text{Im}(\Omega)}. \quad (16)$$

The free-decay frequency and damping in (15) and (16) have been determined numerically from (2). The parameter values used in the calculations are given in table 3.

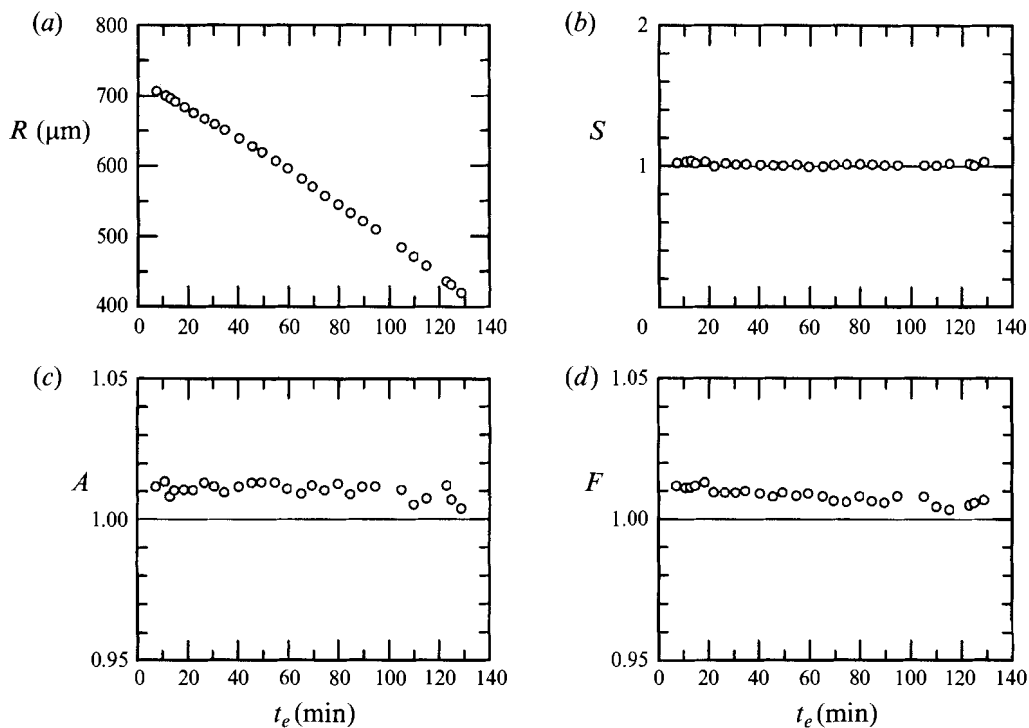


FIGURE 4. Experimental measurements of the physical and dynamic properties of a single air bubble undergoing free decay of quadrupole shape oscillations in clean water (case 1). The quantities depicted are: (a) the volume equivalent radius R ; (b) the ratio of experimental to theoretical damping constant S ; (c) the equilibrium aspect ratio A ; and (d) the ratio of the experimental to theoretical frequency F . Theoretical frequency and damping values were obtained numerically.

5.1. Case 1. Air bubble in clean water

The results of this first example are shown in figure 4. The study was conducted over the course of two hours. The bubble radius decreased from a value of 707 μm to about 420 μm . The dissolution of the bubble shows a remarkably linear decrease in the radius with time. This behaviour is in agreement with previous findings for large acoustically levitated bubbles (Asaki *et al.* 1993), but is fundamentally different than the predicted and observed dissolution of small clean bubbles which show a linear decrease in the surface area with time (Epstein & Plesset 1950; Roesler 1951; Liebermann 1957; Berge 1990). The increased rate of dissolution may be due to gas transport through acoustic streaming. A piece of flat glass was placed on the levitator to prevent water contamination through airborne particulates. Near theoretical damping was observed over the course of the entire experiment. The bubble aspect ratio A remained constant near 1.01. The frequency F was observed to be about 1% above theoretical predictions. This discrepancy will be examined in §6.

5.2. Case 2. Air bubble in clean water

A second example performed for a bubble in clean water illustrates a more complicated behaviour. These results are shown in figures 5 and 6. This bubble was observed to dissolve from a radius of 1400 μm to 430 μm over the course of 66 min. The data for which the bubble has a radius of less than 800 μm shows all of the basic features discussed for case 1. It is apparent from figure 6 that the damping undergoes an abrupt

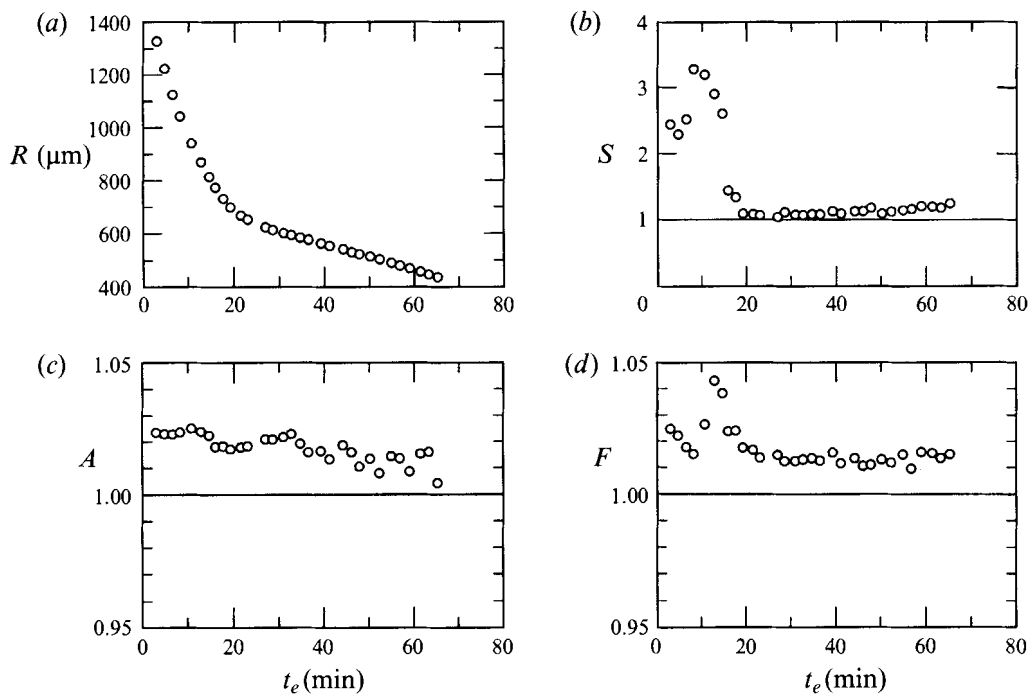


FIGURE 5. Experimental measurements of the physical and dynamic properties of a single air bubble undergoing free decay of quadrupole shape oscillations in clean water (case 2). The quantities depicted are: (a) the volume equivalent radius R ; (b) the ratio of experimental to theoretical damping constant S ; (c) the equilibrium aspect ratio A ; and (d) the ratio of the experimental to theoretical frequency F . Theoretical frequency and damping values were obtained numerically. Note the anomalous large damping for bubbles larger than a critical radius $R_c \approx 800 \mu\text{m}$.

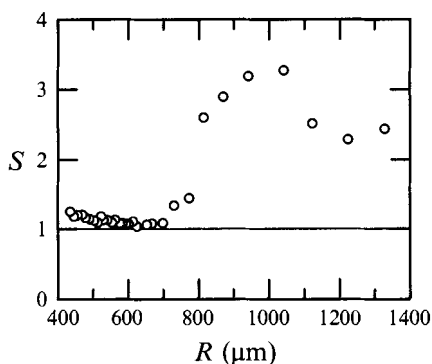


FIGURE 6. Damping ratio S for the bubble of figure 5 plotted as a function of bubble radius R . There is a clear division at a critical radius, $R_c \approx 800 \mu\text{m}$, between anomalous large damping ($S \approx 3$) and near theoretical damping ($S \approx 1$). This transition is characteristic of all bubbles studied in clean liquids and is independent of bubble age.

change at a critical radius, $R_c \approx 800 \mu\text{m}$. At early times ($t_e < 15 \text{ min}$) for which $R > R_c$ the bubble exhibits anomalous large damping values ($S \approx 3$). This effect is observed for all bubbles trapped in clean water and independent of bubble age. Case 1 is an example of a bubble which spent its entire lifetime with a radius less than this critical radius; the anomalous damping is never present. It is not within the scope of

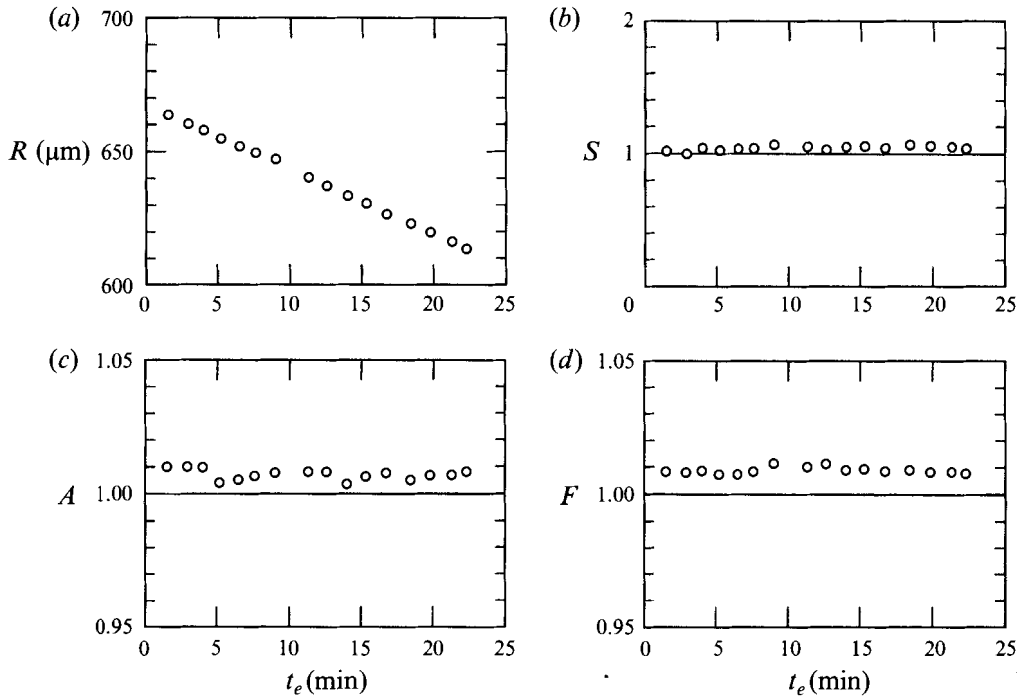


FIGURE 7. Experimental measurements of the physical and dynamic properties of a single air bubble undergoing free decay of quadrupole shape oscillations in clean 0.5 M NaCl solution (case 3). The quantities depicted are: (a) the volume equivalent radius R ; (b) the ratio of experimental to theoretical damping constant S ; (c) the equilibrium aspect ratio A ; and (d) the ratio of the experimental to theoretical frequency F . Theoretical frequency and damping values were obtained numerically. The results are qualitatively similar to those of air bubbles in clean water.

this work to present a detailed study of this phenomena. However, it is important that its characteristics are recognized so that any anomalous damping can be avoided in experiments intended to probe the interfacial damping. The observed features of this phenomena (Asaki 1995) include a steady-state response which is nonlinear in ϵ , the presence of subharmonics in the steady-state frequency spectrum, and a non-exponential free decay. While the origin of the excess damping has not been determined, it is plausible that coupling of energy between different modes of the bubble is related to the cause.

When the bubble radius drops below R_c the damping suddenly drops to near unity. The damping S exhibits a slow increase over time. This may be attributable to the collection and concentration of impurities on the bubble surface. In this example, and in the subsequent examples, no protective glass was placed on the levitator to inhibit possible airborne contamination. The frequency also exhibits initial values near unity and a subsequent slow increase over time. The general behaviour of the damping and frequency at later times is suggestive of the importance of surface elasticity at surfactant concentrations far below those which would significantly affect the static surface tension (Lu & Apfel 1990; Barter 1994). The measured surface tensions of samples of the water before and after the experiment were 72.3 dyn cm^{-1} .

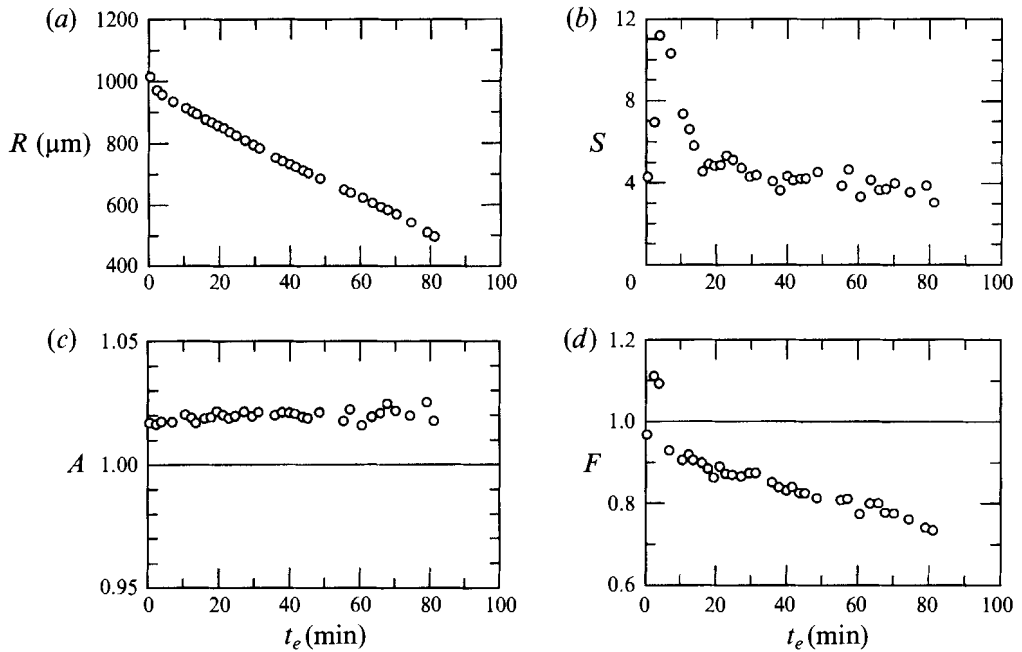


FIGURE 8. Experimental measurements of the physical and dynamic properties of a single air bubble undergoing free decay of quadrupole shape oscillations in sea water (case 4). The quantities depicted are: (a) the volume equivalent radius R ; (b) the ratio of experimental to theoretical damping constant S ; (c) the equilibrium aspect ratio A ; and (d) the ratio of the experimental to theoretical frequency F . Theoretical frequency and damping values were obtained numerically. The results for the frequency and damping are fundamentally different to those observed for clean fluids.

| | Cases 1 and 2 clean water | Case 3 NaCl solution | Case 4 sea water |
|---|------------------------------|-------------------------|---------------------|
| T ($^{\circ}\text{C}$) | 23.1 | 23.5 | 21.4 |
| σ (dyn cm^{-1}) | 72.3 | 73.2 | 73.5 |
| ρ_i (mg cm^{-3}) | 1.082 | 1.081 | 1.089 |
| ρ_o (mg cm^{-3}) | 997.5 | 1018 | 1024 |
| μ_i ($\text{mg s}^{-1} \text{cm}^{-1}$) | 0.184 | 0.184 | 0.184 |
| μ_o ($\text{mg s}^{-1} \text{cm}^{-1}$) | 9.304 | 9.674 | 10.51 |

TABLE 3. Temperature and fluid property values used in the numerical evaluation of (2) for the experiments described in §3. Clean-water values were interpolated from Weast (1985). Salt solution and sea-water values were interpolated from Weast (1985) and Horne (1969). The surface tension for sea water is taken to be that of 0.5 M NaCl.

5.3. Case 3. Air bubble in clean salt water

A third experiment was conducted for a bubble in 0.5 M NaCl solution. This concentration is similar to that of sea water (Horne 1969). The results are shown in figure 7. The bubble was observed for 23 min. The results are qualitatively similar to those of the clean-water cases for $R < R_c$. The radius decreases linearly with time and the aspect ratio remains constant near a value of 1.01. The free decay closely matches the theoretical predictions for the salt solution used.

5.4. Case 4. Air bubble in sea water

A final experiment was performed on an air bubble in sea water. The water sample was obtained from the Colvos Passage of Puget Sound west of Seattle, Washington in March 1994. The water was degassed at about 0.5 atm. for 20 min, but was otherwise untreated and unfiltered before bubble injection. The results are shown in figure 8. The bubble radius decreases linearly in time and the aspect ratio remains constant near 1.02. The free-decay frequency and damping exhibit more complicated behaviours than were seen for the cases involving clean fluids. The damping rises to a value near 11 within 5 min and then slowly decreases over 80 min to a value approaching 3. The frequency F shows an initial rise to a value of 1.1 corresponding to the region of maximum damping. At later times, the frequency decreases and continues to do so for the remainder of the experiment eventually reaching a value near 0.7. The significantly large damping present during the entire bubble lifetime and the complicated behaviour of the frequency suggest the presence of surfactants which create non-ideal interfacial conditions.

6. Conclusion and discussion

The asymptotic expansion for the free decay of shape oscillations of a liquid sphere in an immiscible fluid has been extended. New terms have been shown to be important for describing systems of dissimilar densities and viscosities. Comparisons have been made with numerical calculations. The measured free decay of quadrupole oscillations of an air bubble acoustically trapped in clean water also supports the analysis. Air bubbles in clean water and in salt water exhibit near theoretical frequencies and damping constants; the interface behaves ideally. Work was also presented for the case of an air bubble in sea water which exhibited complicated frequency and damping behaviour indicative of the accumulation of surfactants at the bubble surface.

It is noteworthy that, because of the small size of the bubbles studied, the acoustic field required to trap them did not need to be as large in amplitude as for some of the previous studies (Asaki *et al.* 1993; Asaki & Marston 1994). Large bubbles trapped in large-amplitude standing waves can manifest a standing capillary wave roughening of the surface closer to the pressure antinode in the absence of modulation (see Asaki & Marston (1994) and references cited therein). This complexity was avoided in the experiments described here.

For bubbles in purified water or NaCl solution smaller than the critical size R_c , the observed-to-calculated frequency ratio F deviates from unity by typically 1%, and is similar to the deviation of the aspect ratio A from unity (see figures 4, 5 and 7). This discrepancy may be due to a failure of effective radius procedure, equation (14), to fully account for the acoustic field. For example, the assumed superposition of static and dynamic responses does not include any modification by the acoustic field of the restoring force associated with the quadrupole mode. Previously reported observations of the approximate frequency of maximum response obtained on the Earth (Asaki *et al.* 1993) were for much larger bubbles for which the aspect ratio A is significantly larger. The resulting deviations from predicted frequencies were more significant. It is noteworthy that when a similar experiment was performed with large bubbles on the Space Shuttle on USML-1 in 1992, each bubble was nearly spherical because the radiation pressure needed to trap the bubble was insignificant (Marston *et al.* 1994). For the two large bubbles for which the frequency was measured, the agreement with theory was much better than for similar large bubbles on the Earth (Asaki *et al.* 1993).

The observation of this paper that weak static deformation is needed for improved agreement with theory is consistent with the results from USML-1.

This work was supported by the United States Office of Naval Research.

Appendix A. Complex free decay frequency expansion

The characteristic determinant, equation (2), can be reduced by considering the asymptotic expansions for complex Bessel and Hankel functions, ratios of large argument which appear in the boundary conditions. These expansions are:

$$\mathcal{Q}_l^h \equiv \frac{h_{n+1}^{(1)}(z_o)}{h_n^{(1)}(z_o)} \approx -i + \frac{n+1}{z_o} + i \frac{n(n+1)}{2z_o^2} + \frac{n(n+1)}{2z_o^3} + i \frac{(n-2)n(n+1)(n+3)}{8z_o^4} + \dots, \quad (\text{A } 1)$$

$$\mathcal{Q}_l^j \equiv \frac{j_{l+1}(z_i)}{j_l(z_i)} \approx i + \frac{n+1}{z_i} - i \frac{n(n+1)}{2z_i^2} + \frac{n(n+1)}{2z_i^3} - i \frac{(n-2)n(n+1)(n+3)}{8z_i^4} + \dots \quad (\text{Re}(z_i) > 0), \quad (\text{A } 2)$$

$$\mathcal{Q}_l^j \approx -i + \frac{n+1}{z_i} + i \frac{n(n+1)}{2z_i^2} + \frac{n(n+1)}{2z_i^3} + i \frac{(n-2)n(n+2)(n+3)}{8z_i^4} + \dots \quad (\text{Re}(z_i) < 0), \quad (\text{A } 3)$$

where $h_n^{(1)}(z_o)$ and $j_n(z_i)$ are the spherical Hankel function of the first kind and the spherical Bessel function, respectively, both of order n . The complex $z_i(z_o)$ is seen in (5) to be proportional to the ratio of the radius to the inner (outer) thickness of the oscillating boundary layer. The simplified characteristic, equation (6), is obtained by substitution of equations (A 1)–(A 3) into equation (2) and retention of the highest-order Ω terms.

The parameters α , γ and κ are given by

$$\alpha = \frac{(2n+1)^2 a_o a_i}{\sqrt{2R}\Gamma(a_o + a_i)}, \quad (\text{A } 4)$$

$$\gamma = \frac{(2n+1)(M_1 a_o^2 + M_2 a_i^2)}{R^2 \Gamma(a_o + a_i)^2}, \quad (\text{A } 5)$$

$$\kappa = \frac{2a_o a_i (M_1 a_o - M_2 a_i)^2 - (a_o + a_i)(M_3 a_o^3 + M_4 a_i^3)}{2\sqrt{2}\Gamma R^3 a_o a_i (a_o + a_i)^3}. \quad (\text{A } 6)$$

The following notation has been used:

$$a_o \equiv (\rho_o \mu_o)^{1/2}, \quad a_i \equiv (\rho_i \mu_i)^{1/2}, \quad (\text{A } 7)$$

$$M_1 = 2n(n+2)\mu_o - (n-1)\mu_i, \quad (\text{A } 8)$$

$$M_2 = (n+2)\mu_o + 2(n-1)(n+1)\mu_i, \quad (\text{A } 9)$$

$$M_3 = (2n+1)^2(n+1)(n+2)\mu_i^2, \quad (\text{A } 10)$$

$$M_4 = (2n+1)^2 n(n-1)\mu_o^2. \quad (\text{A } 11)$$

The expressions for α and γ are the same as those first calculated by Miller & Scriven (1968). When the two fluids are dissimilar, κ is a positive quantity. However, for fluids of similar densities and viscosities κ can be negative. The next term in the characteristic equation δ has not been explicitly calculated.

Radiative and thermal losses associated with the monopole oscillations of bubbles in water has been considered by Devin (1959). Marston (1980) has estimated that for

shape oscillations radiative losses (based upon the work of Strasberg 1956) are negligible in comparison to viscous contributions. The effect of any temperature gradients associated with shape oscillations should be weak and have been neglected in the analysis.

Appendix B. Frequency of maximum response

The frequency of maximum response for driven oscillations ω^{max} can be calculated numerically (or approximated) by

$$\frac{\partial}{\partial \omega} \left| \frac{C}{D} \right|_{\omega^{max}} = 0, \quad (\text{B } 1)$$

where D is the determinant in equation (2) and C is the minor of D given by:

$$C = (z_i \mathcal{Q}_n^j) [-\mu_o z_o^2 + 2(2n+1)\mu_o - 2\mu_o z_o \mathcal{Q}_n^h] - (2n+1 - z_o \mathcal{Q}_n^h) (-\mu_i z_i^2 + 2\mu_i z_i \mathcal{Q}_n^j). \quad (\text{B } 2)$$

Leading-order terms have been calculated by Marston & Goosby (1985). Inclusion of the leading-order κ term gives the expression

$$\omega^{max} \approx \omega - \frac{\alpha\omega^{1/2}}{2} - \frac{5\alpha\gamma}{8\omega^{1/2}} + \frac{\kappa}{2\omega^{1/2}} - \frac{\gamma^2}{4\omega}. \quad (\text{B } 3)$$

Comparison of this expression with numerical results is provided in table 1 for the case of an air bubble in water. Calculations based on (B 3) compare favourably with numerical solutions of (B 1). Note also that the frequency of maximum response is very nearly equal to the free-decay frequency.

REFERENCES

- ASAKI, T. J. 1995 Shape oscillations of bubbles in water driven by modulated ultrasonic radiation pressure and applications to interfacial dynamics. PhD thesis, Washington State University.
- ASAKI, T. J. & MARSTON, P. L. 1994 Acoustic radiation force on a bubble driven above resonance. *J. Acoust. Soc. Am.* **96**, 3096–3099.
- ASAKI, T. J. & MARSTON, P. L. 1995 Equilibrium shape of an acoustically levitated bubble driven above resonance. *J. Acoust. Soc. Am.* **97**, 2138–2143.
- ASAKI, T. J., MARSTON, P. L. & TRINH, E. H. 1993 Shape oscillations of bubbles in water driven by modulated ultrasonic radiation pressure: observations and detection with scattered laser light. *J. Acoust. Soc. Am.* **93**, 706–713.
- BARTER, J. D. 1994 Surface strain modulation of insoluble surface film properties. *Phys. Fluids* **6**, 2606–2616.
- BERGE, L. I. 1990 Dissolution of air bubbles by the resistive pulse and the pressure reversal technique. *J. Colloid Interface Sci.* **134**, 548–562.
- CRUM, L. A. 1994 Sonoluminescence, sonochemistry, and sonophysics. *J. Acoust. Soc. Am.* **95**, 559–562.
- DEVIN, C. 1959 Survey of thermal, radiation, and viscous damping of pulsating air bubbles in water. *J. Acoust. Soc. Am.* **31**, 1654–1667.
- EPSTEIN, P. S. & PLESSET, M. S. 1950 On the stability of gas bubbles in liquid–gas solutions. *J. Chem. Phys.* **18**, 1505–1509.
- HORNE, R. A. 1969 *Marine Chemistry*. John Wiley & Sons.
- HSU, C. J. & APFEL, R. E. 1985 A technique for measuring interfacial tension by quadrupole oscillation of drops. *J. Colloid Interface Sci.* **107**, 467–476.
- HSU, C. J. & APFEL, R. E. 1987 Model for the quadrupole oscillations of drops for determining interfacial tension. *J. Acoust. Soc. Am.* **82**, 2135–2144.

- LAMB, H. 1932 *Hydrodynamics*. Dover.
- LIEBERMANN, L. 1957 Air bubbles in water. *J. Appl. Phys.* **28**, 205–211.
- LONGUET-HIGGINS, M. S. 1992 Nonlinear damping of bubble oscillations by resonant interaction. *J. Acoust. Soc. Am.* **91**, 1414–1422.
- LU, H. & APFEL, R. E. 1990 Quadrupole oscillations of drops for studying interfacial properties. *J. Colloid Interface Sci.* **134**, 245–255.
- MARSTON, P. L. 1980 Shape oscillation and static deformation of drops and bubbles driven by modulated radiation stresses – Theory. *J. Acoust. Soc. Am.* **67**, 15–26.
- MARSTON, P. L. & APFEL, R. E. 1979 Acoustically forced shape oscillation of hydrocarbon drops levitated in water. *J. Colloid Interface Sci.* **68**, 280–286.
- MARSTON, P. L. & APFEL, R. E. 1980 Quadrupole resonance of drops driven by modulated acoustic radiation pressure – Experimental properties. *J. Acoust. Soc. Am.* **67**, 27–37.
- MARSTON, P. L. & GOOSBY, S. G. 1985 Ultrasonically stimulated low-frequency oscillation and breakup of immiscible liquid drops: Photographs. *Phys. Fluids* **28**, 1233–1242.
- MARSTON, P. L., TRINH, E. H., DEPEW, J. & ASAKI, T. J. 1994 Response of bubbles to ultrasonic radiation pressure: dynamics in low gravity and shape oscillations. In *Bubble Dynamics and Interface Phenomena: Proceedings of an IUTAM Symposium* (ed. J. R. Blake, J. M. Boulton-Stone & N. H. Thomas), pp. 343–353. Kluwer.
- MILLER, C. A. & SCRIVEN, L. E. 1968 The oscillations of a fluid droplet immersed in another fluid. *J. Fluid Mech.* **32**, 417–435.
- MONAHAN, E. C. & VAN PATTEN, M. A. (eds.) 1989 *The Climate and Health Implications of Bubble-Mediated Sea–Air Exchange. Proceedings*. Connecticut Sea Grant.
- PROSPERETTI, A. 1980a Normal-mode analysis for the oscillations of a viscous liquid drop in an immiscible liquid. *J. Méc.* **19**, 149–182.
- PROSPERETTI, A. 1980b Free oscillations of drops and bubbles: the initial-value problem. *J. Fluid Mech.* **100**, 333–347.
- ROESLER, F. C. 1951 Comment on ‘Gas bubbles in solutions’. *J. Chem. Phys.* **19**, 512–513.
- SCOTT, J. C. 1978 In *Surface Contamination: Genesis, Detection, and Control*, vol. 1, pp. 477–497. Plenum.
- STRASBERG, M. 1956 Gas bubbles as sources of sound in liquids. *J. Acoust. Soc. Am.* **28**, 20–26.
- STROUD, J. S. & MARSTON, P. L. 1993 Optical detection of transient bubble oscillations associated with the underwater noise of rain. *J. Acoust. Soc. Am.* **94**, 2788–2792.
- STROUD, J. S. & MARSTON, P. L. 1994 Transient bubble oscillations associated with the underwater noise of rain detected optically and some properties of light scattered by bubbles. In *Bubble Dynamics and Interfacial Phenomena: Proc. IUTAM Symp.* (ed. J. R. Blake, J. M. Boulton-Stone & N. H. Thomas), pp. 161–169. Kluwer.
- TRINH, E. H., MARSTON, P. L. & ROBEY, J. L. 1988 Acoustic measurement of the surface tension of levitated drops. *J. Colloid Interface Sci.* **124**, 95–103.
- TRINH, E. H., ZWERN, A. & WANG, T. G. 1982 An experimental study of small-amplitude drop oscillations in immiscible liquid systems. *J. Fluid Mech.* **115**, 453–474.
- WEAST, R. C. (ed.) 1985 *CRC Handbook of Chemistry and Physics*. CRC Press.
- YANG, S. M., FENG, Z. C. & LEAL, L. G. 1993 Nonlinear effects in the dynamics of shape and volume oscillations for a gas bubble in an external flow. *J. Fluid Mech.* **247**, 417–454.
- YOUNG, F. R. 1989 *Cavitation*. McGraw-Hill.